Article

Seeding as a Decisive Tool for Increasing Space-Time-Yields in the Preparation of High-Quality Cu/ZnO/ZrO₂ Catalysts

David Guse [1], Lucas Warmuth [2], Moritz Herfet [2], Katharina Adolf [1], Thomas A. Zevaco [2], Stephan Pitter [2] and Mat-thias Kind [1,*]

[1] Karlsruhe Institute of Technology, Institute of Thermal Process Engineering, Engler-Bunte-Ring 21, 76131 Karlsruhe, Germany

[2] Karlsruhe Institute of Technology, Institute of Catalysis Research and Technology, Engler-Bunte-Ring 21, 76131 Karlsruhe, Germany

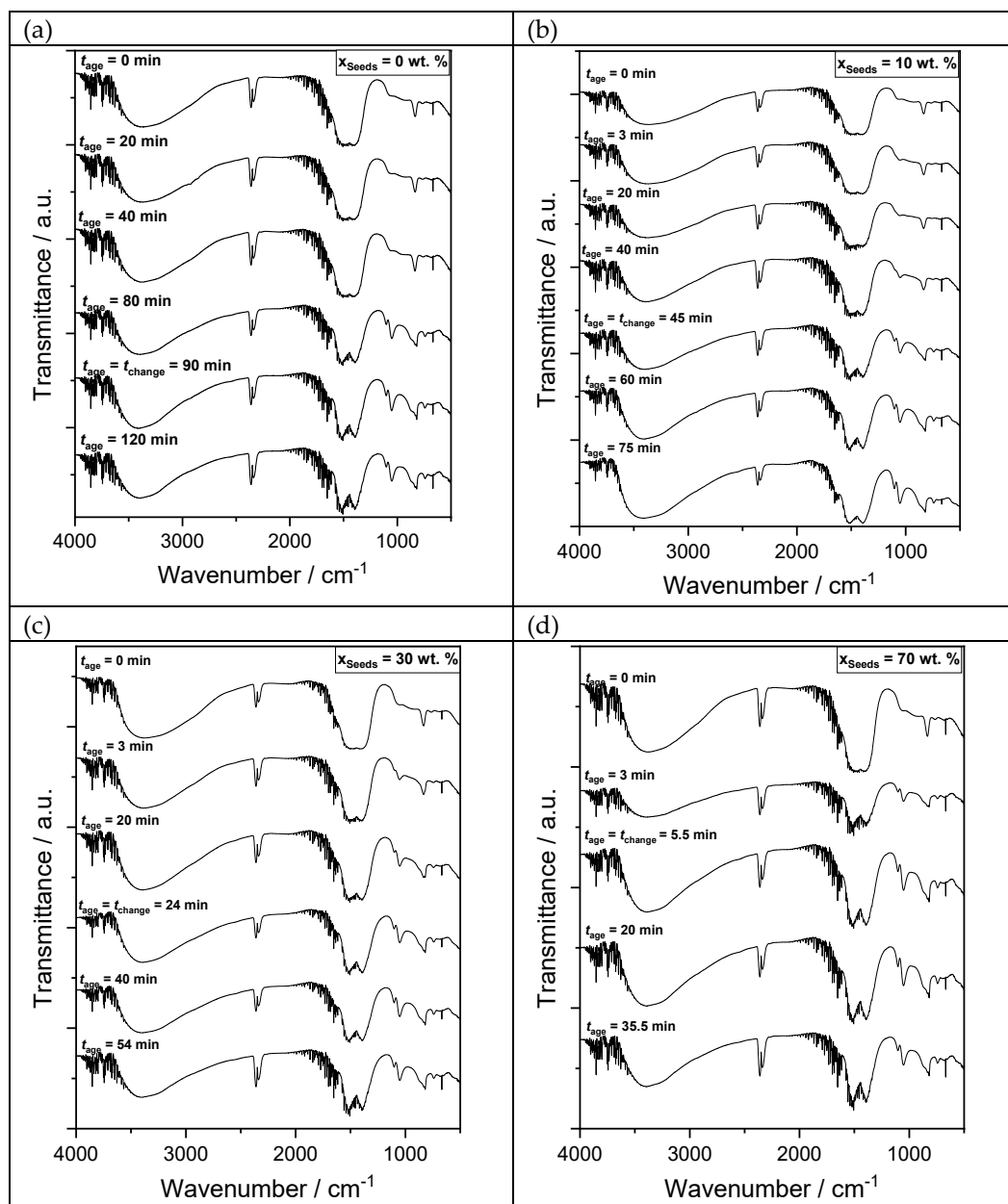* Correspondence: matthias.kind@kit.edu (MK)

Supporting Information

1. FT-IR analysis during aging

In Figure S1, the FT-IR spectra as a function of aging over time are compared for an unseeded preparation and three seeded preparations with varying x_{Seeds}, offered as a complementary analysis to the XRD evaluation, which is unable to identify which amorphous phase is present.

In general, the major absorption bands at 834 cm⁻¹ and 1474 cm⁻¹ are present in all samples and can both be attributed to (zincian) georgeite in the literature if the XRD diffractogram indicates an amorphous structure, or to (zincian) malachite if the material is crystalline [41,83]. They are the result of out-of-plane O-C-O bending modes [31] and asymmetric C-O stretching, respectively [84]. The small peak at 668 cm⁻¹ can be attributed to rosasite [31] and C-O vibrations [65]. The large absorption band at around 3400 cm⁻¹, which is present in all samples, can be attributed to O-H [65]. This is most probably the result of adsorbed water from the atmosphere during sample preparation with hygroscopic KBr discs.

For each preparation, three major differences in the spectra are present when comparing the amorphous samples for $t_{\text{age}} \ll t_{change}$ with the crystalline samples for $t_{\text{age}} \geq t_{\text{change}}$: the main absorption band shifts from 1480 to 1500 cm⁻¹, which was observed in the literature when the phase transformation of zincian georgeite to zincian malachite is completed [34,83,84]. Additionally, the second absorption band at around 1415 to 1380 cm⁻¹ grows markedly [34]. Lastly, additional peaks appear for wavenumbers below 1200 cm⁻¹ [31].
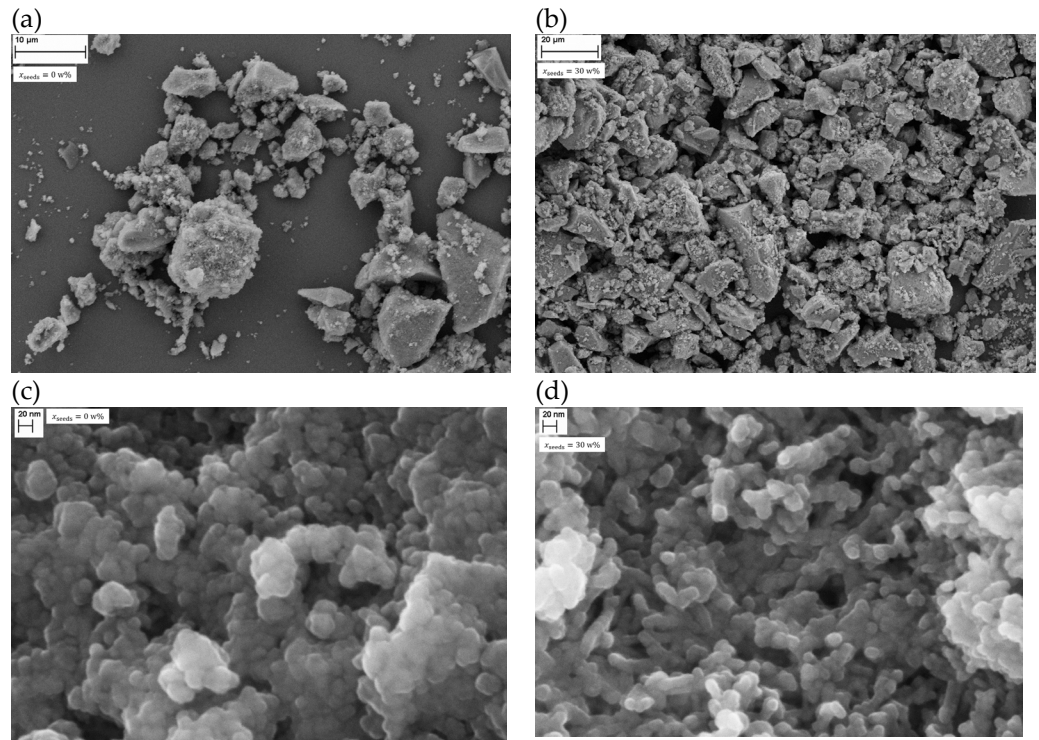
In summary, the analysis of the FT-IR spectra confirms the assumption drawn from the XRD diffractograms that, first, zincian georgeite forms and, second, transforms into zincian malachite. The more seeds consisting of zincian malachite that are present in the suspension, the shorter the induction time becomes for this phase transformation.

Figure S1. FT-IR spectra of the dried and washed samples as a function of aging time for: **(a)** a standard aging process without seeding ($x_{Seeds} = 0\ wt.\%$), **(b)** a preparation where seeds were added after co-precipitation is completed at $t_{age} = 0\ min$ ($x_{Seeds} = 10\ wt.\%$), **(c)** $x_{Seeds} = 30\ wt.\%$ and **(d)** $x_{Seeds} = 70\ wt.\%$.
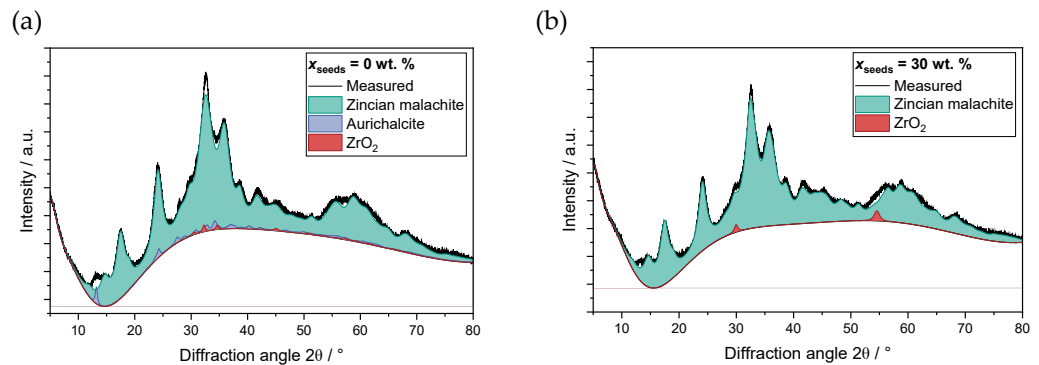
2. Supplementary analysis of the aged precursor

Figure S2 shows the SEM images of two aged precursors from unseeded (left) and seeded ($x_{Seeds} = 30\ wt.\%$, right) aging at two different magnifications. Both the overview image and the detail shot show a very similar morphology in either case. This implies that the reduced aging time that results from seeding does not influence the morphology.

Figure S2. SEM images of two aged precursors from unseeded $(x_{seeds} = 0\ wt.\%)$ **(a)** and **(c)** and seeded $(x_{seeds} = 30\ wt.\%)$ **(b)** and **(d)** aging, respectively, at two magnifications.

The X-ray diffractograms in Figure S3 show the measured data for an unseeded sample (a) and a seeded sample, with $x_{seeds} = 30\ wt.\%$ (b). In both cases, the Rietveld refinement results in zincian malachite as the predominant phase, where $x_{zm} > 99$ wt.%. This implies that seeding does not influence the phase composition after the phase change is completed.

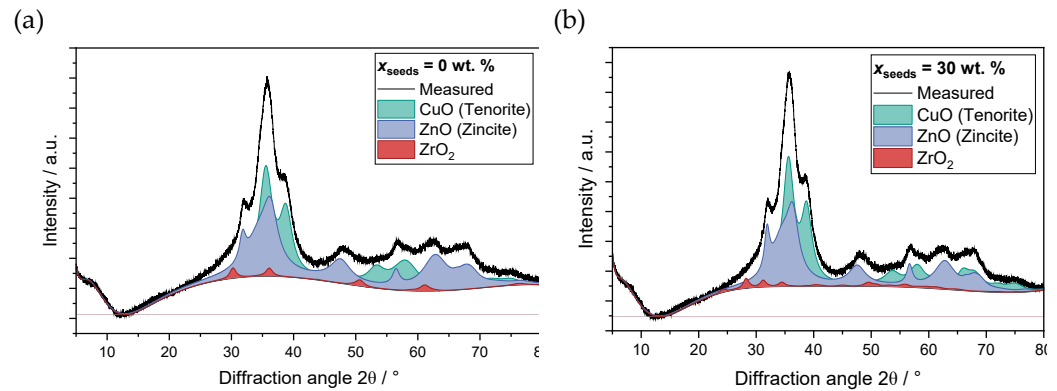**Figure S3.** X-ray diffractograms of two aged precursors from unseeded $(x_{seeds} = 0\ wt.\%)$ **(a)** and seeded $(x_{seeds} = 30\ wt.\%)$ **(b)** aging, showing the measured diffractogram in black and the phases determined by Rietveld refinement in color.

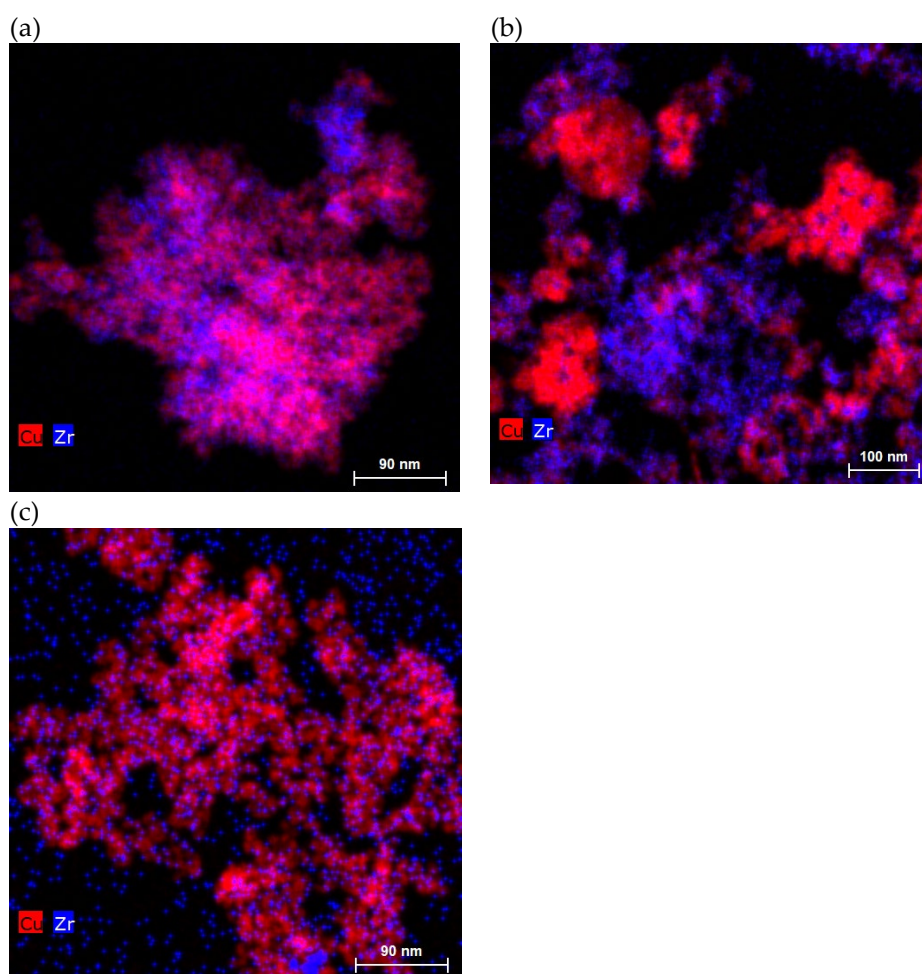## 3. Supplementary analysis of the calcined precatalyst

The X-ray diffractograms in Figure S4 show the measured data of two calcined precatalysts from an unseeded (a) and a seeded (b) aging process. In both cases, the Rietveld refinement results in a mixture of tenorite and zincite (CuO and ZnO) as the two predominant phases. The position and overlap of the respective peaks make quantitative phase evaluation difficult and prone to errors. Altogether, the evaluation indicates that

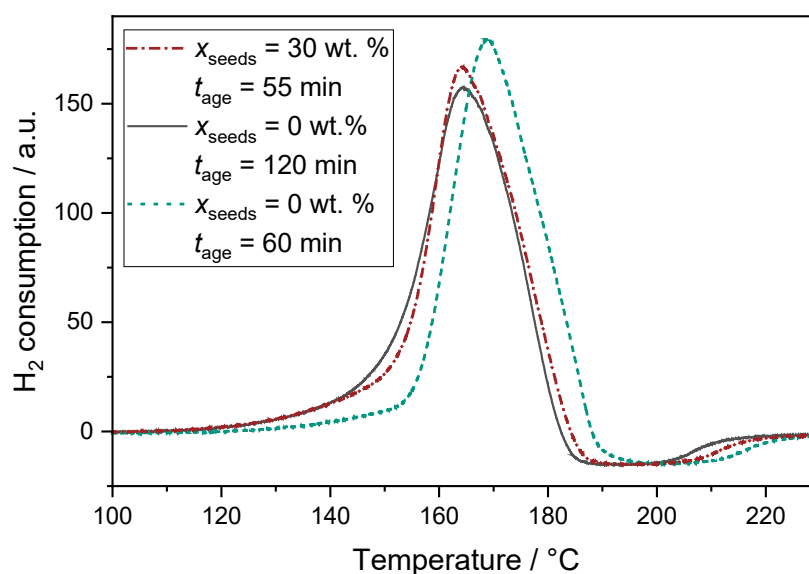seeding does not influence the phase composition of the calcined material after calcination is completed.

(a)　　　　　　　　　　　　　　　　　　　　(b)

Figure S4. X-ray diffractograms of two calcined precatalysts from unseeded $(x_{seeds} = 0\,wt.\%)$ **(a)** and seeded $(x_{seeds} = 30\,wt.\%)$ **(b)** aging, showing the measured diffractogram in black and the phases determined by Rietveld refinement in color.

Figure S5 shows TEM-EDXS images of three calcined precatalysts, with highlighted Cu and Zr distribution from an unseeded (a) preparation, an unseeded preparation with a reduced aging time (b) and seeded aging (c). The section corresponds to the section shown in Figure 9. For the first and last samples, it is evident that Cu and Zr are distributed homogeneously. However, for the unseeded sample with a reduced aging time, separate regions for Cu and Zr are evident, which indicates an inhomogeneous material. This observation matches the distribution of Cu and Zn in Figure 9 (main text) for the same sample. Thus, while a sufficiently long aging time is necessary for homogeneous material in general, seeding does not influence the metal distribution if $t_{age} > t_{change}$ is valid.

Figure S5. TEM-EDXS images of the calcined precatalysts for **(a)** the unseeded preparation at $t_{age} = 122$ min, **(b)** the unseeded preparation with a shortened aging step ($t_{age} = 60$ min) and **(c)** a seeded preparation ($x_{seeds} = 30$ wt.%) with a shortened aging step ($t_{age} = 55$ min). Cu is marked in red and Zr is marked in blue. The Zn distribution is shown in Figure 9.

The comparison of the H_2-TPR profiles in Figure S6 shows that both the unseeded preparation and the seeded preparation once the phase change was completed ($t_{age} = 122$ min) show the same onset temperature for reduction, as well as the same maximum position. In contrast, both the onset and the maximum are shifted toward higher temperatures for the unseeded preparation with a shortened aging time ($t_{age} = 60$ min) and no phase change. This confirms the impact of the phase transformation during the aging step on the product properties and, likewise, the importance of seeding to maintain product properties despite reducing the total aging time.

Figure S6. H_2-TPR profiles of the chosen precatalysts.

The Altamira AMI-300 used for the TPR and N_2O pulse chemisorption analyses is equipped with four mass flow controllers, which are responsible for the relevant four inlet groups: carrier, treatment, blend and auxiliary. The chemisorption equipment was piloted via the proprietary steering software (AMI 300) found in the Altamira software package, whereas the evaluation of the TPR and N_2O pulse chemisorption profiles was performed using AMI-Analysis.

The samples were first dried under argon at 120 °C (flow 30 ml/min; temperature ramp 10 K/min; holding 30 min at 200 °C) followed by cooling down to 50 °C under Ar flow (20 K/min). The temperature was raised afterward from 50 °C to 250 °C at a rate of 1 K/min (250 °C holding for 45 min) in a gas mixture containing 5 vol% H_2/Ar (10 vol% H_2/Ar Air Liquide CRYSTAL gas mixture at 15 ml/min and pure Ar at 15ml/min). The TCD was calibrated before the experiment began, using the same diluted 5% H_2/Ar gas mixture (flow 30 ml/min; 5 pulses; volume of the loop, 518 µl).

The pulse chemisorption was performed using a gas mixture of 5 vol% N_2O in helium (using a 10 vol% N_2O/He Air Liquide CRYSTAL gas mixture at 15 ml/min and pure helium at 15 ml/min). Prior to taking the measurements, the system had to be thoroughly flushed with pure helium (15 min, 30 ml/min, 50 °C). Once in a steady state, the sample was subjected to 60 pulses of N_2O, alternating pure helium (30 ml/min) and N_2O/He pulses. The liberated N_2 pulses measured with the TCD showed a typical "comb" pattern, with the active surface being gradually and mildly oxidized to completion. The relatively high number of pulses, combined with a low N_2O loading, allowed for good precision of measurement, almost similar to the reactive frontal chromatography (RFC) method performed with continuous flow, very low N_2O loadings (1–2 vol% N_2O in He) and, typically, an MS detector. The TCD was calibrated with each measurement.

3. Materials and methods: additional information

The pH electrode was calibrated daily with two reference solutions (KAY0.1, Roth and KAY1.1, Roth for $4 < pH < 7$ or KAY1.1, Roth and KAY2.1, Roth for $7 < pH < 10$), the choice of which depended on the expected pH profile during aging. The conductivity meter was calibrated with two reference solutions (conductivity standards 1413 ± 1 µS/cm and 84 ± 1 µS/cm, Carl Roth GmbH).

For the Rietveld refinement, the following reference data were applied: malachite (BGMN [77]), modified according to Guse et al. [46], hydrozincite (BGMN), aurichalcite (RRUFF ID R060426.1), $Na_2Zn_3(CO_3)_4 \cdot 3H_2O$ (ICSD 81305), ZrO_2 (ICSD 83862 and 18190),

β-Zr(OH)$_2$(NO$_3$)$_2$·5(H$_2$O) (ICSD 84658), Zr(OH)$_3$NO$_3$ (ICSD 80062), CuO (04-007-1375, Ceramics, Profex) and Zincite (BGMN).

For the ICP-OES analyses, 50–100 mg of solid sample was first digested in 6 ml of 65% HNO$_3$ and 2 ml of 30% HCL solution in a microwave heat oven (Multiwave 3000, Anton Paar) for 2 hours at a maximum pressure of 60 bar and at 240 to 250 °C. Then, the sample was diluted to a total of 50 ml with ultrapure water (≤ 0.75 μS·cm^{-1}) and analyzed. The ICP-OES reference solutions VHG-MISA6-500 (VHG Labs) and ICP Mehrelement-standardlösung IV (Carl Roth GmbH) were applied for calibration.

For DLS analysis, the suspension was diluted by a ratio of 1:10 with demineralized water, placed in a single-use cuvette (Y194.1, Carl Roth) and analyzed in a Zetasizer Nano ZS (Malvern Panalytical). Dilution of the suspension was necessary to prevent multi-refraction of the different particles and agglomeration and to obtain a high signal-to-noise ratio [78]. A refractive index of 1.655 [71], the literature value for malachite, and an absorption index of 0.3 [80] were used. For SLS, the sample suspension was diluted with demineralized water until the specifications for the obscuration level were met and then pumped in circulation through the measurement cell (Mastersizer 3000 with Hydro EV, Malvern Panalytical) [79]. The same material data as were used for the DLS measurements were applied. Additionally, the particle size and morphology were validated by SEM evaluation.

4. References

41.   Zhang, Q.-C.; Cheng, K.-P.; Wen, L.-X.; Guo, K.; Chen, J.-F. A Study on the Precipitating and Aging Processes of CuO/ZnO/Al 2 O 3 Catalysts Synthesized in Micro-Impinging Stream Reactors. *RSC Adv.* **2016**, *6*, 33611–33621, doi:10.1039/C6RA02512A.

83.   Shen, G.-C.; Fujita, S.; Matsumoto, S.; Takezawa, N. Steam Reforming of Methanol on Binary CuZnO Catalysts: Effects of Preparation Condition upon Precursors, Surface Structure and Catalytic Activity. *Journal of Molecular Catalysis A: Chemical* **1997**, *124*, 123–136, doi:10.1016/S1381-1169(97)00078-2.

31.   Behrens, M.; Girgsdies, F.; Trunschke, A.; Schlögl, R. Minerals as Model Compounds for Cu/ZnO Catalyst Precursors: Structural and Thermal Properties and IR Spectra of Mineral and Synthetic (Zincian) Malachite, Rosasite and Aurichalcite and a Catalyst Precursor Mixture. *Eur. J. Inorg. Chem.* **2009**, *2009*, 1347–1357, doi:10.1002/ejic.200801216.

84.   Fujita, S.; Satriyo, A.M.; Shen, G.C.; Takezawa, N. Mechanism of the Formation of Precursors for the Cu/ZnO Methanol Synthesis Catalysts by a Coprecipitation Method. *Catal Lett* **1995**, *34*, 85–92, doi:10.1007/BF00808325.

65.   Kondrat, S.A.; Smith, P.J.; Wells, P.P.; Chater, P.A.; Carter, J.H.; Morgan, D.J.; Fiordaliso, E.M.; Wagner, J.B.; Davies, T.E.; Lu, L.; et al. Stable Amorphous Georgeite as a Precursor to a High-Activity Catalyst. *Nature* **2016**, *531*, 83–87, doi:10.1038/nature16935.

34.   Pollard, A.M.; Spencer, M.S.; Thomas, R.G.; Williams, P.A.; Holt, J.; Jennings, J.R. Georgeite and Azurite as Precursors in the Preparation of Co-Precipitated Copper/Zinc Oxide Catalysts. *Applied Catalysis A: General* **1992**, *85*, 1–11, doi:10.1016/0926-860X(92)80125-V.